Optics Letters

Intelligently optimized digital optical phase conjugation with particle swarm optimization

ZHONGTAO CHENG, JIAMIAO YANG, AND LIHONG V. WANG*

Caltech Optical Imaging Laboratory, Andrew and Peggy Cherng Department of Medical Engineering, Department of Electrical Engineering, California Institute of Technology, Pasadena, California 91125, USA
**Corresponding author: LVW@caltech.edu*

Received 4 November 2019; revised 7 December 2019; accepted 8 December 2019; posted 9 December 2019 (Doc. ID 381930); published 10 January 2020

Wavefront shaping (WFS) based on digital optical phase conjugation (DOPC) has gained major interest in focusing light through or inside scattering media. However, the quality of DOPC is greatly limited by imperfections of the system in a complicated and coupled way. In this Letter, we incorporate the concept of global optimization to solve this problem comprehensively for the first time, to the best of our knowledge. An automatic and intelligent optimization framework for DOPC techniques is proposed, leveraging the global optimization ability of particle swarm optimization (PSO). We demonstrate the general and powerful ability of the proposed approach in a series of DOPC-related experiments for focusing through and inside scattering media. This novel work can improve the OPC quality greatly and simplify the development of a high-performance DOPC system, which may open up a new avenue for the general scientific community to benefit from DOPC-based WFS in their potential applications.

https://doi.org/10.1364/OL.381930

The advent of optical wavefront shaping (WFS) techniques in recent years brings a new possibility for conquering light scattering in applications such as optical imaging, photodynamic therapy, and optical manipulations deep inside biological tissues. We can roughly divide WFS into three categories: feedback-based iterative WFS [1–3], transmission matrix inversion [4–6], and optical phase conjugation (OPC) [7–13]. Among them, OPC features the advantages of high speed. OPC can be implemented in two ways: analog OPC (AOPC) [7–10] and digital OPC (DOPC) [11–16]. Because of the intrinsic capability to achieve a fluence reflectivity greater than unity, DOPC has sparked major interest in focusing light through or inside scattering media for some applications [17,18]. DOPC employs a digital camera to measure the phase information of scattered light through interferometry. Based on the measured phase, a spatial light modulator (SLM) is used to modulate a plane wave as the conjugated field of the scattered light. Although straightforward in principle, the practical implementation of DOPC is actually complicated system engineering. Achieving a good OPC quality imposes stringent requirements on the system for the phase measurement of the scattered field and the generation of the conjugated wavefront [18,19]. Unfortunately, it is inevitable to introduce imperfections into the system because of optical aberration, mechanical misalignment, and even the curvature of the SLM itself. The quality of the OPC is largely limited by these imperfections in a complicated and coupled way. Separate correction for these imperfections are actually less effective and even troublesome [18]. Moreover, frequent realignment is found to be necessary on a day-to-day basis for the optimal DOPC performance because the accumulative mechanical drift or environmental disturbance may severely degrade the system capacity. All these aspects make the building and maintaining of a DOPC system challenging, which limits DOPC to be only an exclusive technique for optical experts in this realm rather than a general tool to benefit a broader community as it should be.

Here, we incorporate the concept of global optimization to solve these problems comprehensively for the first time. Leveraging the global optimization ability of particle swarm optimization (PSO), we propose an automatic and intelligent optimization framework for DOPC techniques. The PSO intelligently explores the Zernike mode space to optimally determine and compensate for the imperfections of a DOPC system. Because the PSO is implemented experimentally on the basis of the physical system, it has the inherent ability to correct system imperfections well. Without the loss of generality, most of the DOPC systems can be considered as a variant of the basic experimental setup shown in Fig. 1. The scattered light from the scattering medium (SM) is collected through the lens L3 and interferes with a plane reference beam at the beam splitter (BS) BS2 (Laser, Verdi G5, Coherent). The interferogram is reflected on the surface of the SLM (Pluto-2-VIS, Holoeye) and relayed to the camera (PCO.edge 5.5, PCO) plane by the BS3 and camera lens (CL). Note that the SLM and the camera are at a pair of conjugated positions with a calibrated pixel match relationship. In addition, the light incident on the SLM should be horizontally polarized because this SLM is only sensitive for this polarization direction. In the experiments, the phase of the scattered beam is retrieved through the heterodyne phase-shifting interferometry first, and, next, its conjugated phase map is loaded to the SLM. The phase-modulated playback beam reflected back by the SLM becomes the time-reversed version of

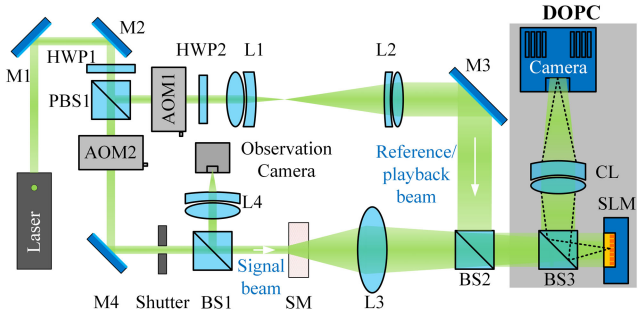

Fig. 1. Experimental setup for the general DOPC system. AOM, acousto-optic modulator; BS, beam splitter (nonpolarizing); CL, camera lens; HWP, half-wave plate; L, lens; M, mirror; PBS, polarizing beam splitter; SLM, spatial light modulator; SM, scattering media.

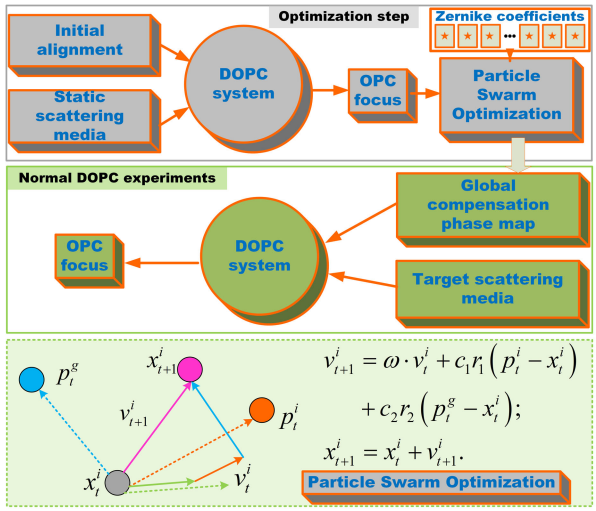

Fig. 2. Schematic illustration of the proposed PSO-based optimization framework for DOPC techniques.

the scattered light, and can retrace its trajectory through the SM. We can verify the OPC quality by focusing the time-reversed beam onto the observation camera (Grasshopper 3, FLIR) using a lens (L4).

We outline the proposed PSO-based optimization framework for DOPC techniques in Fig. 2. In the optimization step, an experiment for focusing through a static SM should be conducted to launch the optimization process, such that the decorrelation of the SM is negligible during the optimization period. After a DOPC system is initially aligned using conventional approaches, the OPC focus can generally be seen on the observation camera, although the intensity may not be optimal because of the system's imperfections. Starting with this OPC focus, self-tuning of the system is performed by iteratively adjusting the Zernike coefficients of a compensation phase map that is added to the conjugated phase of the scattered field and loaded to the SLM in each iteration. The optimal phase Zernike coefficients are searched through PSO until the intensity of the OPC focus converges to the maximum. Then a global compensation phase map is generated corresponding to the optimal Zernike coefficients from the PSO, and stored in the computer as the parameters of the DOPC system. Next, we can start the normal DOPC experiments using any desirable SM as the target. The global compensation phase map is superposed to the conjugated phase map of the speckle field in each experiment to cancel the system's imperfections. In this way, an optimally improved OPC focus is obtained.

The PSO is a population-based intelligent computational method that globally optimizes a problem by iteratively updating some candidate solutions with respect to a target feedback signal [20,21]. In our problem here, the candidate solution is the Zernike coefficients related to the global compensation phase, and the feedback is the intensity of the OPC focus in the optimization step. PSO is launched from a randomly initiated population, called particle swarm. Each particle position in the swarm corresponds to a possible solution of the target problem. PSO updates each particle position x^i_t in the swarm iteratively according to a velocity vector v^i_{t+1}, where i is the particle index and t is the current iteration number. The velocity vector v^i_{t+1} incorporates three kinds of information: the velocity vector in the last iteration v^i_t, the individual best position p^i_t, and the global best position of the whole swarm p^g_t as of the tth iteration (see the vector graph in Fig. 2). The importance of this information is weighted by factors ω, c_1, and c_2, which are the inertia weight, self-adjustment weight, and social-adjustment weight, respectively. The inertia weight controls the impact of the previous history of velocities on the current velocity, and generally is set to decrease linearly with time. r_1 and r_2 are two uniformly [0,1] distributed random vectors. Compared with most modern optimization methods, PSO features many desirable advantages simultaneously such as few parameters to be tuned, good global searching ability, and fast convergence. Here, we employ the concept of PSO to realize our optimization framework for DOPC techniques.

We illustrate the proposed method in more detail with an experimental example in Fig. 3. Here, we use two optical diffusers (DG-220, Thorlabs) to start the optimization step. After carefully aligning the system conventionally, the initial OPC focus through the SM can be obtained, as shown in Fig. 3(b). Next, we perform the PSO to search for the global compensation phase map using the intensity of the OPC focus as feedback and the coefficients of the second through 10th rectangular Zernike modes [22] as optimization variables. The Zernike modes with higher orders are found to have less influence on the DOPC [19]. In our PSO configuration, the swarm size is set to 50, the self-adjustment weight and social-adjustment weight are both set to 1.49, and the inertia weight range is set to [0.1 1.1]. Instead of initiating the particle positions completely randomly, here we designate one of the particles in the swarm as **0**. In this way, we can launch the PSO from the current system alignment, rather than from a completely random state. A typical intensity curve of the OPC focus during the optimization is presented in Fig. 3(c). We can see that the PSO starts to converge after about 40 generations, and the intensity of the OPC focus increases greatly at the end of iterations. After the optimization step is completed, the final OPC focus is acquired, as shown in Fig. 3(d). The peak-to-background ratio (PBR) of the OPC focus, which is defined as the ratio of the peak intensity of the OPC focus to the mean intensity of the speckle pattern when a random phase map is loaded to the SLM, increases from the original 1.15×10^4 to 9.46×10^4. The Zernike coefficients of the global compensation phase from the PSO in this experiment are given in Fig. 3(e) while the corresponding global compensation phase is shown in Fig. 3(f).

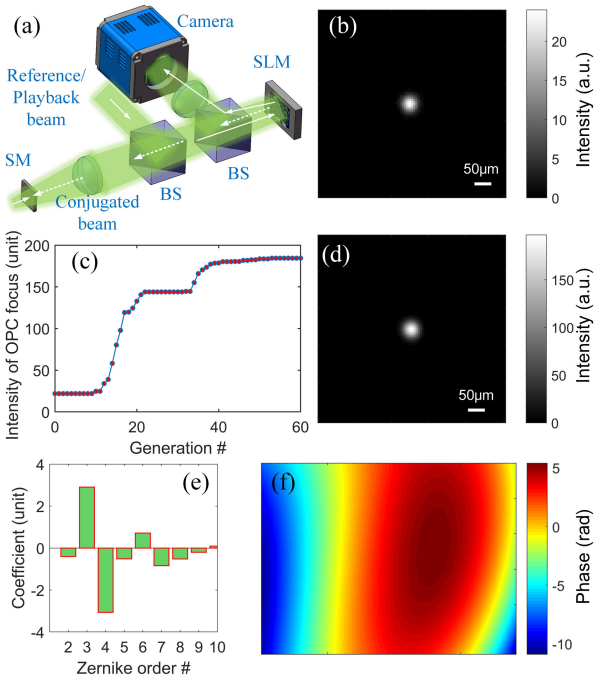

Fig. 3. Experimental realization of the particle swarm optimization for a DOPC system. (a) Simplified schematic of the DOPC system on the basis of Fig. 1; (b) OPC focus for focusing through a static scattering medium before the PSO process; (c) intensity of the OPC focus during the PSO updating process; (d) final result of the OPC focus after the PSO process; (e) Zernike coefficients of the global compensation phase in this experiment searched via the PSO; (f) corresponding global compensation phase map.

After obtaining the global compensation phase map via the PSO in the optimization step above, we can use it to improve the system performance with any SM as the target in the DOPC experiments. To demonstrate this point, we change the SM in Fig. 3 into three optical diffusers. The OPC focus without loading the global compensation phase to the SLM is shown in Fig. 4(a1), with a PBR of 1.17×10^4. After adding the global compensation phase into the conjugated phase of the speckle field, the PBR of the OPC focus [Fig. 4(a2)] increases to 8.92×10^4 immediately. We also show another group of experimental results using a 2 mm thickness chicken tissue as the SM in Figs. 4(b1)–4(b2). Similar to Figs. 4(a1)–4(a2), the OPC foci before and after the global compensation phase map obtained via the PSO is incorporated are presented in Figs. 4(b1) and 4(b2), respectively. The PBR increases from 347 to 2235 in this case.

The proposed scheme is also effective for focusing light inside scattering media. Below, we will demonstrate its applications in two different DOPC-based focusing-inside modalities, that is, the time-reversed adapted-perturbation (TRAP) optical focusing [23] and the time-reversed ultrasonically encoded (TRUE) optical focusing [8,12]. In short, the TRAP and TRUE methods focus light inside scattering media by taking advantage of different "guide star" mechanisms. The guide star of TRAP is the dynamic perturbations inside the scattering media (e.g., absorption or refractive index change) while that of TRUE is the ultrasonic focus of an externally applied ultrasonic field.

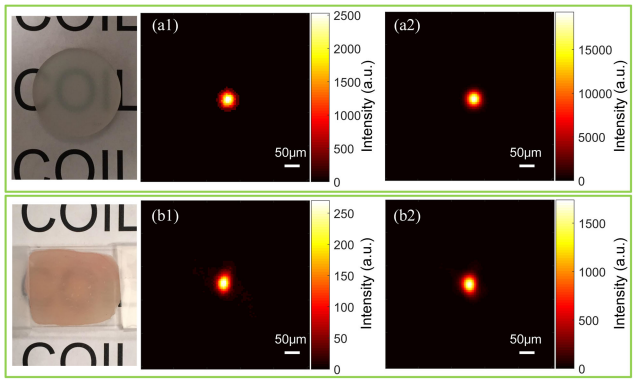

Fig. 4. Applications of the proposed method to DOPC for focusing through general scattering media. (a1)–(a2) OPC foci (a1) before and (a2) after the global compensation phase from the PSO is superposed to the conjugated phase of the scattered filed when using three optical diffusers as the scattering medium. The PBR increases from 11,700 to 89,200. (b1)–(b2) Same as (a1)–(a2) correspondingly except that the experiments are performed using a 2 mm thickness chicken tissue as the scattering medium. The PBR increases from 347 to 2235.

In the TRAP optical focusing experiment [23], a piece of human hair, which is mounted on a rotatable motor, is sandwiched between two optical diffusers separated by a distance of ∼ 10 cm to mimic the dynamic perturbation inside tissues [Fig. 5(a)]. We rotate the hair to two different positions and measure the scattered field at each position. Then, the conjugated phase of the complex differential field is calculated

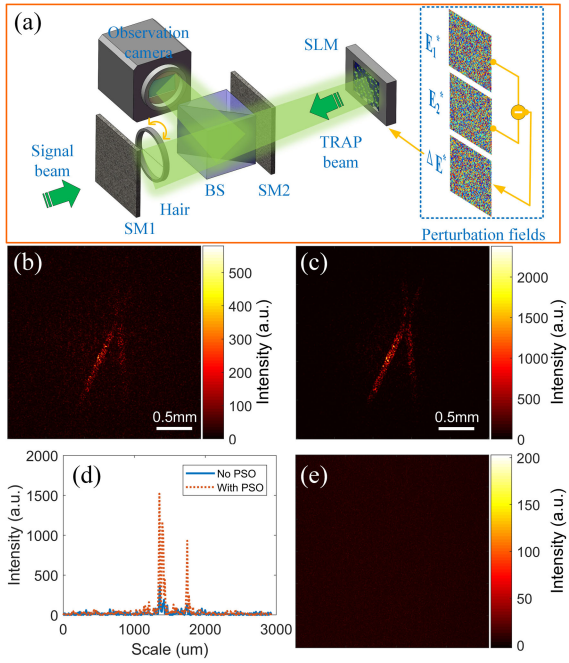

Fig. 5. Application of the proposed method to TRAP optical focusing. (a) Simplified schematic of the TRAP optical focusing experiment; (b) and (c) focused patterns inside the scattering medium (b) before and (c) after the global compensation phase from the PSO is added into the conjugated phase of the scattered field. The PBR increases to 438 from the original 107. (d) Line profiles of the central rows of (b) and (c) for a better comparison. (e) No focused pattern can be seen when a random phase map is displayed on the SLM.

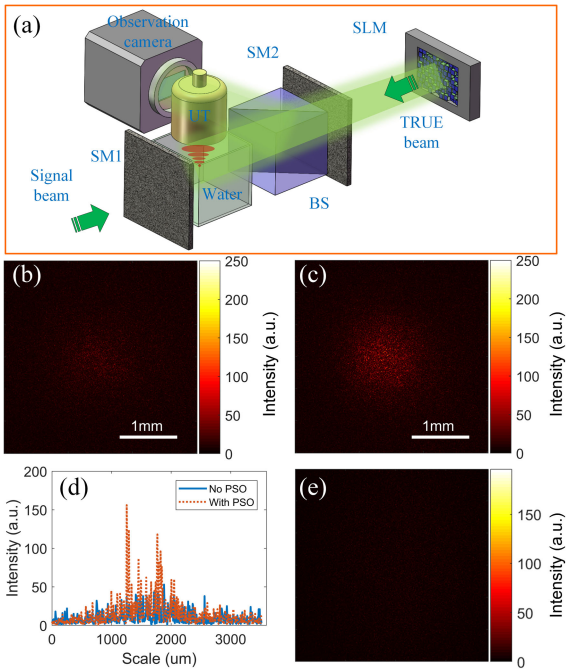

Fig. 6. Application of the proposed method to TRUE optical focusing. (a) Simplified schematic of the TRUE optical focusing experiment; (b) and (c) TRUE foci inside the scattering medium (b) before and (c) after the global compensation phase obtained via the PSO is added into the conjugated phase of the scattered field. The PBR increases to 52 from the original 26. (d) Line profiles of the central rows of (b) and (c) for a better comparison. (e) No focus can be seen when a random phase map is displayed on the SLM or the frequency of the signal beam is detuned by 100 kHz. UT, ultrasound transducer.

and loaded to the SLM. To visualize the focused pattern conveniently, a BS is inserted between the two diffusers to pick up a copy of the playback beam to the observation camera. Figure 5(b) shows the focused pattern before the global compensation phase map from the PSO is loaded to the SLM. Although we can see clearly the TRAP pattern resulted from the perturbation of the hair, the intensity of the focus is not high, and there exist severe background speckles around the focused pattern. After adding the global compensation phase map obtained via the PSO into the conjugated phase of the scattered light, a much brighter TRAP pattern is obtained, and the surrounding background speckles are attenuated greatly [Fig. 5(c)]. The PBR increases to 438 from the original 107.

In the TRUE optical focusing experiment [8,12] [Fig. 6(a)], an ultrasound focus is produced using an ultrasound transducer (A381S, Panametrics, USA) to shift the frequency of the scattered light. We record the interferograms resulted from the interference between the frequency-shifted photons and the reference beam. Then the conjugated phase of these ultrasound-tagged photons is retrieved based on the interferograms and is displayed on the SLM to generate the TRUE beam, which can trace back to the position of the ultrasound focus. In Fig. 6(b), we show the TRUE focus observed on the observation camera without using our PSO approach. After the global compensation phase map from the PSO is loaded to the SLM, the TRUE focus becomes much brighter immediately, as shown in Fig. 6(c). The PBR increases to 52 from the original 26.

We point out that all these experiments shown in Figs. 4–6 use the same global compensation phase map from Fig. 3. For our PSO configuration, an optimization process takes ∼ 20 min, which is mainly limited by the low communication speed between the instruments (camera and SLM) and the control program. Of course, because the PSO only needs to be carried out for one time before the normal DOPC experiments, the optimization time is not a limitation for the DOPC technique itself. In conclusion, the proposed optimization framework for the DOPC techniques via the automatic and intelligent PSO method provides a general and powerful tool to improve the OPC quality and simplify the development and maintenance of a high-performance DOPC system. With the proposed optimization framework, the PBRs that we realize in this work are much higher (at least 5 times higher) than those reported in previous elaborate works on similar experimental conditions [11,23,24]. Besides the PSO, other global optimization strategies can also be incorporated into our DOPC optimization framework.

Funding. National Institutes of Health (R01 CA186567).

Disclosures. The authors declare no conflicts of interest.

REFERENCES

1. H. Frostig, E. Small, A. Daniel, P. Oulevey, S. Derevyanko, and Y. Silberberg, Optica **4**, 1073 (2017).
2. I. M. Vellekoop and A. P. Mosk, Opt. Lett. **32**, 2309 (2007).
3. P. Lai, L. Wang, J. W. Tay, and L. V. Wang, Nat. Photonics **9**, 126 (2015).
4. S. M. Popoff, G. Lerosey, R. Carminati, M. Fink, A. C. Boccara, and S. Gigan, Phys. Rev. Lett. **104**, 100601 (2010).
5. M. Jang, Y. Horie, A. Shibukawa, J. Brake, Y. Liu, S. M. Kamali, A. Arbabi, H. Ruan, A. Faraon, and C. Yang, Nat. Photonics **12**, 84 (2018).
6. M. Mounaix, D. Andreoli, H. Defienne, G. Volpe, O. Katz, S. Grésillon, and S. Gigan, Phys. Rev. Lett. **116**, 253901 (2016).
7. Z. Yaqoob, D. Psaltis, M. S. Feld, and C. Yang, Nat. Photonics **2**, 110 (2008).
8. X. Xu, H. Liu, and L. V. Wang, Nat. Photonics **5**, 154 (2011).
9. Y. Liu, P. Lai, C. Ma, X. Xu, A. A. Grabar, and L. V. Wang, Nat. Commun. **6**, 5904 (2015).
10. Z. Cheng, J. Yang, and L. V. Wang, Appl. Phys. Lett. **114**, 231104 (2019).
11. Y. Shen, Y. Liu, C. Ma, and L. V. Wang, Optica **4**, 97 (2017).
12. Y. Liu, C. Ma, Y. Shen, J. Shi, and L. V. Wang, Optica **4**, 280 (2017).
13. D. Wang, E. H. Zhou, J. Brake, H. Ruan, M. Jang, and C. Yang, Optica **2**, 728 (2015).
14. Z. Yu, J. Huangfu, F. Zhao, M. Xia, X. Wu, X. Niu, D. Li, P. Lai, and D. Wang, Sci. Rep. **8**, 2927 (2018).
15. A. S. Hemphill, Y. Shen, J. Hwang, and L. V. Wang, J. Biomed. Opt. **24**, 031004 (2018).
16. Z. Yu, M. Xia, H. Li, T. Zhong, F. Zhao, H. Deng, Z. Li, D. Li, D. Wang, and P. Lai, Sci. Rep. **9**, 1537 (2019).
17. K. Si, R. Fiolka, and M. Cui, Nat. Photonics **6**, 657 (2012).
18. H. Ruan, J. Brake, J. E. Robinson, Y. Liu, M. Jang, C. Xiao, C. Zhou, V. Gradinaru, and C. Yang, Sci. Adv. **3**, eaao5520 (2017).
19. J. Yang, J. Li, S. He, and L. V. Wang, Optica **6**, 250 (2019).
20. E. Mezura-Montes and C. A. Coello Coello, Swarm Evol. Comput. **1**, 173 (2011).
21. K. R. Harrison, B. M. Ombuki-Berman, and A. P. Engelbrecht, *IEEE Congress on Evolutionary Computation (CEC)* (2017), p. 349.
22. V. N. Mahajan and G.-M. Dai, J. Opt. Soc. Am. A **24**, 2994 (2007).
23. C. Ma, X. Xu, Y. Liu, and L. V. Wang, Nat. Photonics **8**, 931 (2014).
24. Y. Shen, Y. Liu, C. Ma, and L. V. Wang, Opt. Lett. **41**, 1130 (2016).